

Probing Individual Molecules with Confocal Fluorescence Microscopy

Shuming Nie,* Daniel T. Chiu, Richard N. Zare†

Confocal fluorescence microscopy coupled with a diffraction-limited laser beam and a high-efficiency detection system has been used to study the diffusive movement and emission process of individual fluorescent molecules in the liquid phase at room temperature. The high detection sensitivity achieved at fast data acquisition speeds (greater than 1 kilohertz) allows real-time observation of single-molecule fluorescence without statistical analysis. The results show fluorescence-cycle saturation at the single-molecule level and multiple recrossings of a single molecule into and out of the probe volume as well as the triplet state.

The detection and characterization of a single molecule represents the ultimate goal in ultrasensitive chemical analysis. The ability to directly visualize individual molecules has applications that span physical and biological sciences. We report a simple method that combines laser excitation, confocal microscopy, and avalanche photodiode detection for studying individual dye molecules in solution. The achieved sensitivity is so high that we can study in detail the fluorescence cycle as a single molecule repeatedly emits photons while it is present in the small probe volume being interrogated. Conventional measurements of molecular dynamics and reactions in the condensed phase represent averages over large numbers of molecules and events. Following an individual molecule in real time allows an understanding of dynamical behavior at a level of detail that can reveal new features buried in the statistical averaging.

Single molecules have been detected in the condensed phase by various means. In low-temperature crystalline hosts, Mörner (1) and Orrit *et al.* (2) demonstrated single-molecule detection and spectroscopy through spectral isolation of individual molecules in the wings of an inhomogeneously broadened line by using frequency-modulated absorption and laser-induced fluorescence. Diffraction-limited optics also permits the two-dimensional detection of a single molecule embedded in low-temperature solids (3) and on mirrorlike silicon wafer surfaces (4). Near-field optical microscopy has been used by Betzig and Chichester (5) and Trautman *et al.* (6) to study individual carbocyanine molecules fixed on thin polymer films at room temperature. In liquids, single-molecule fluorescence detection has been achieved for rhodamines and phycoerythrins in a hydrodynamic flow cell (7, 8) and in levitated microdroplets (9). Eigen

and Rigler (10) recently showed the detection and manipulation of individual rhodamine 6G molecules (R6G) in water by using fluorescence correlation spectroscopy (11) coupled with a confocal microscope and devices for trapping single molecules in an electric field. Biological macromolecules (that is, DNA) labeled with more than one fluorescent tag have also been visualized and manipulated at the single-molecule level with fluorescence microscopy through attachment to dielectric (12) and magnetic (13) beads, by the dielectrophoresis effect (14), during gel electrophoresis (15, 16), and in free solution (17, 18). Furthermore, single molecules of RNA polymerase have been observed with light microscopy sliding and transcribing along a DNA chain (19, 20).

This report describes the use of far-field confocal fluorescence microscopy at the optical diffraction limit for probing individual molecules in the liquid phase, that is, molecules in motion. Through the use of a high-efficiency photon detection system, we examine in detail the diffusive movement and emission characteristics of a single molecule as well as the photophysical behavior of a single-chromophore molecule in solution. We also report the first detection of individual fluorescein molecules in aqueous media and the extraordinary detection sensitivity achieved for common fluorescent dyes in various sampling environments. In a preliminary study, we have detected single DNA bases labeled with one fluorescent tag and observed in real time gyration radius changes for individual large DNA fragments (~2000 bp).

The confocal fluorescence microscopy system is based on a Nikon Diaphot inverted microscope (21). The probe volume is limited latitudinally by optical diffraction and longitudinally by spherical aberration of the objective. The diffraction-limited radius is calculated to be 250 to 260 nm under our experimental conditions (TEM₀₀ laser beam radius 0.65 mm, objective focal length 1.6 mm, and a laser wavelength

488.0 or 514.5 nm). The $1/e^2$ probe depth (z_0) is primarily determined by spherical aberration of the objective and has been experimentally measured to be ~1.0 μm (22, 23). In our experiment, the cylindrical probe volume, $\pi r_0^2(2z_0)$, is estimated to be $\sim 5.0 \times 10^{-16}$ liters or 0.5 fl. At a concentration of 3.3×10^{-9} M, this probe volume contains an average of only one molecule, that is, an equal probability of 0.37 for finding zero or one molecule and 0.18 for finding two molecules in the probe volume. By choosing to work at lower concentrations, we can observe almost exclusively single-molecule events. Aggregated molecular clusters might be expected to show similar behaviors as single molecules, but dilution studies we have made ruled out this possibility as the source of our observed signal at low dye concentrations.

Several measures were taken to maximize the overall (combined) detection efficiency. First, an oil-immersion, high-numerical-aperture (NA 1.3) objective lens was used to collect ~20% of the emitted fluorescence photons. Second, a photon-counting Si avalanche photodiode was used for high-efficiency detection. Third, signal attenuation in the optical path was minimized by using as few optical elements as possible. For example, only one interference bandpass filter was used to reject the laser light, Rayleigh scattering, Raman scattering, and impurity fluorescence. The overall detection efficiency of our confocal fluorescence system was 0.5 to 1.0%, a value considerably higher than that reported in hydrodynamic flow (7, 8) but comparable to that in near-field optical microscopy (5, 6). Samples (10 μl) were transferred onto a microscope cover glass (0.13-mm thick). A second cover glass was placed immediately on top to prevent solvent evaporation and to produce a thin sample layer between the two cover slips. Best results were obtained when the laser beam was focused at the lower sample-glass interface because spherical aberration of the oil-immersion objective was minimized at this focal point. When the laser beam was focused deep into the sample, spherical aberration became significant owing to the refractive index mismatch between the sample ($n = 1.33$) and the immersion oil ($n = 1.52$).

In solution, fluorescence emission from a single molecule occurs in a four-step cycle: (i) electronic transition from the ground state to an excited state, the rate of which is a linear function of excitation power; (ii) internal relaxation in the excited electronic state; (iii) radiative or nonradiative decay from the excited state to the ground state, which is controlled by the excited state lifetime; and (iv) internal relaxation in the ground state. Vibrational and rotational relaxation generally occurs on the picosecond

Department of Chemistry, Stanford University, Stanford, CA 94305, USA.

*Present address: Department of Chemistry, Indiana University, Bloomington, IN 47405, USA.

†To whom correspondence should be addressed.

time scale for small molecules in the condensed phase, whereas the excited state lifetime and the absorption time are in the subnano- to nanosecond range. Consequently, the fluorescence cycle is primarily determined by the absorption and emission steps. At low power levels, the absorption time is expected to be the dominant factor and the observed fluorescence intensity is approximately linear with laser power. At intermediate power levels, the absorption time becomes comparable to the excited state lifetime and the signal is weakly dependent on power. At high power levels, the absorption time becomes much shorter than the excited state lifetime and the signal is determined by the molecule's intrinsic excited state lifetime and is thus essentially independent of laser power.

This analysis provides the criteria to ascertain if the observed fluorescence signals are truly single-molecule events and are not artifacts such as dust scattering. These criteria can be summarized as: (i) the observation of single-molecule detection events depends on analyte concentration, and its frequency is determined by a Poisson distribution; (ii) the signal intensity depends on the nature of the solvent and on the pH (quantum yield and photostability); (iii) the fluorescence intensity dependence on excitation intensity shows saturation (even for a single molecule); and (iv) the observed number of fluorescence photons does not exceed that expected from the fluorescence cycle of a single molecule.

The time-dependent fluorescence signals observed from aqueous and nonaqueous solutions of rhodamine 6G with 1-ms integration is shown in Fig. 1. The observed jumps in signal intensity are consistent with Poisson statistics (24), which predicts that for a 5.0×10^{-11} M dye solution the 0.5-fl probe volume contains zero dye molecules (background) for 98.5% of the time and one dye molecule (signal) for 1.5% of the time. The probability for zero to two or one to two jumps in the number of molecules is negligibly small. The fluorescence signals show a distribution in intensity and are influenced by the nature of the solvent. The excited state lifetime and absorption properties of R6G are similar in ethanol and water, but its quantum yield decreases from 0.95 in ethanol to ~ 0.45 in water (25). This decrease leads to a substantially lower signal in water, which is confirmed experimentally. Another interesting point is that the R6G signals are essentially independent of solution pH, whereas intense fluorescence signals from fluorescein molecules are observed only at $\text{pH} > 8$ (Fig. 2). This difference is consistent with the fact that the fluorescence of fluorescein, but not R6G, is highly sensitive to pH (caused by a reconfiguration of its π -electron system upon deprotonation).

Photobleaching of R6G molecules does not appear to be significant during the ~ 1 -ms transit time, and the use of protecting agents such as mercaptoethanol has little effect on signal intensity. This behavior is apparently attributable to the high photostability of rhodamine dyes. In contrast, the fluorescence intensity of fluorescein increases significantly in the presence of mercaptoethanol (100 mM), whose protecting effect may arise from its abilities to scavenge oxidative species involved in photobleaching. These results together with dilution studies provide strong evidence that the detected fluorescence signals represent single-molecule events. We have also achieved single-molecule detection for 2',7'-dichlorofluorescein, tetramethylrhodamine, carbocyanines, and boradipyromethane dyes as well as fluorescently labeled proteins, nucleotides, and DNA primers.

A single-molecule detection event starts with a molecule entering the probe volume and ends upon its exit. If not photobleached, the same molecule may reenter the laser beam and generate another detection event. Indeed, Figs. 1 and 2 (see in-

serts) show a clustering effect in the observed single-molecule signals. Considering that the probe volume remains "empty" (zero dye molecules) most of the time, a clustering of detection events indicates that once a molecule diffuses close to the laser beam it may move in and out of the probe volume several times before eventually diffusing away, that is, the same molecule is being multiply detected. The recurrence frequency decreases rapidly with increasing multiplicity (26), consistent with the random walk theory (24). The insert to Fig. 1 shows a rare occasion in which the same molecule is detected five times.

We note that the fluorescence intensity measurement is biased toward molecules that spend a longer period of time in the probe volume because it is a time-integrated technique. The observed detection events are thus dominated by molecules that have long paths (trajectories) in the probe volume. The diffusion time of these molecules can be estimated by the time for traversing the laser beam diameter ($\sim 0.5 \mu\text{m}$), which is calculated to be 0.45 ms (27). This analysis agrees fairly well with the observed average time spread of 0.7 ms for single-molecule events in water and ethanol solution. We stress that the achieved detection efficiency is so high that it allows real-time observation of single-molecule fluorescence without statistical analysis. Contrast this with fluorescence correlation spectroscopy (10, 23, 28), which measures intensity fluctua-

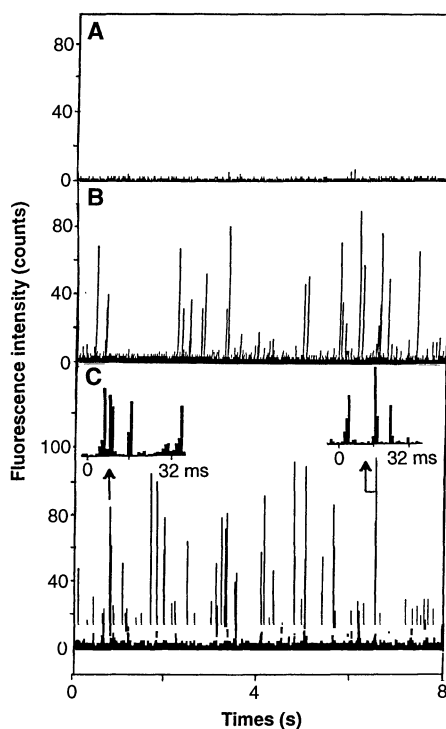


Fig. 1. Time-dependent fluorescence signals observed from aqueous and ethanol rhodamine 6G solution. The inserts are closeup views of the peaks indicated, showing the multiple detection of a single molecule: (A) blank; (B) 2×10^{-11} M rhodamine 6G in water; and (C) 5×10^{-11} M rhodamine 6G in ethanol. The data were acquired at a speed of 1000 data points per second (1-ms integration) and with 0.7-mW laser excitation (514.5 nm). The emission bandpass filter was centered at 560 nm [full-width at half-maximum (FWHM) of 40 nm].

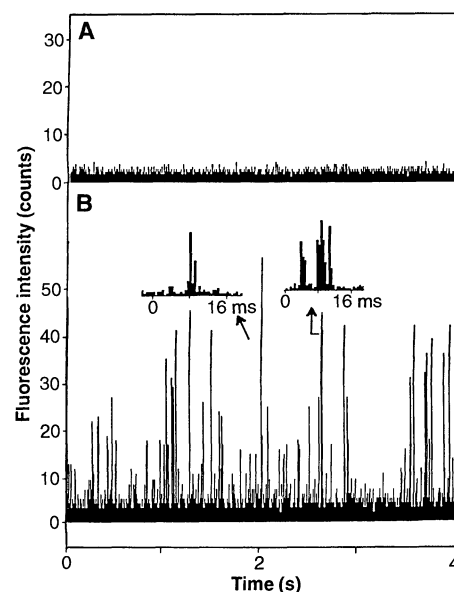


Fig. 2. Detection of individual fluorescein molecules in aqueous 100 mM mercaptoethanol solution ($\text{pH} 12$). The inserts show expanded views of the designated peaks: (A) blank and (B) 3×10^{-10} M fluorescein in water [$\text{pH} 12$; laser wavelength, 488.0 nm; excitation power, 0.2 mW; emission bandpass filter, 530 nm (FWHM 60 nm); and integration time per data point, 0.5 ms].

tuations integrated over an observation time and analyzes the accumulated data statistically.

At the single-molecule level, the fluorescence intensity dependence on excitation intensity is determined by the time it takes the molecule to complete the four-step fluorescence cycle. Figure 3 compares the experimental and calculated intensity dependence on laser power for single R6G molecules in ethanol. The observed three regions (that is, the approximately linear, absorption-dominated region; the transition region; and the saturated, emission-dominated region) are in agreement with theoretical calculations. Similar behaviors are observed for individual fluorescein molecules, except that the emission-dominated region is reached at much lower powers. This result is expected from the larger absorption cross section of fluorescein at 488 nm compared with that of R6G at 514.5 nm.

Figure 4 depicts the time profiles of photon emission obtained from individual R6G molecules at different excitation powers. The results show the detection of predominantly single-photon events with 2- μ s integration and 0.5 to 1.0% combined detection efficiency. The time spread of the photon bursts is approximately 0.5 to 0.8 ms, consistent with the diffusion analysis above.

The temporal relation between the observed and the true photon emission process of a single molecule is complicated in that only a small percentage of the emitted photons are detected. The observation of distinctly short and long "dark periods" between adjacent photons, however, may be caused by two types of phenomena. Intersystem crossing into and out of the triplet state appears to play a role in the observed

short dark periods because their average duration (4 to 6 μ s) at 0.6 mW illumination is comparable to the triplet state lifetime (\sim 4.0 μ s). The longer dark periods show an average duration of 50 μ s, the time expected and simulated for diffusional recrossings of the probe volume periphery by a single molecule. Most detection events show zero to three long dark periods and rarely four or more, consistent with the expected recurrence frequency (24). Thus, our observations indicate a single molecule may multiply traverse the probe volume on the millisecond time scale and recross the probe volume periphery on the microsecond time scale.

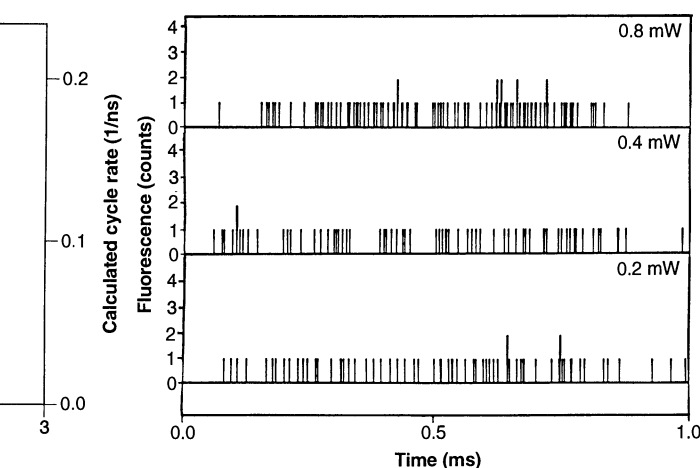
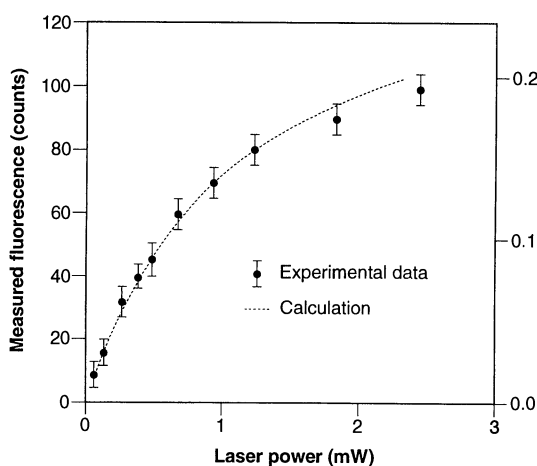
Further evidence for the involvement of the triplet state is that the observed fluorescence signals (50 to 200 photons) are substantially lower than the calculated value (650 to 1300 photons with 1-mW power and 1-ms integration). With a triplet lifetime of \sim 4.0 μ s and an intersystem crossing efficiency of \sim 0.2% (29, 30), a R6G molecule upon excitation is expected to reside in the triplet state for \sim 50% of the time, thereby reducing the calculated fluorescence intensity to 325 to 650 photons. The triplet effect alone is insufficient to account for the observed low fluorescence intensity. We note that additional signal losses are caused by the decreased laser intensity and confocal collection efficiency for a molecule that moves away from the object plane or the optical axis (31). Other factors not included in the calculation are photobleaching and saturation of the fluorescence cycle in the central region of a gaussian laser beam; both are expected to reduce the fluorescence intensity of a single molecule.

An important finding of this work is that

the background level (which arises from 1.5×10^{10} solvent molecules, 5×10^7 electrolyte molecules, and many impurity molecules) is only \sim 6 counts with 1-ms integration, which is negligible compared with the typical fluorescence signal (\sim 100 counts) from single fluorescent dye molecules. The shot noise is therefore the limiting factor, yielding a signal-to-noise (peak-to-peak) ratio of approximately 10 with 1-ms integration. This calculation shows that detection at the single-molecule limit can be achieved with reduced laser intensities, or with shorter integration times, or for molecules having lower fluorescence quantum yields than dye molecules. As a test, we conducted an experiment in which a neutral density filter (optical density = 2.0) was used to block 99% of the fluorescence signal. The results show single-molecule events can still be observed by detecting only 1% of the signal. Consequently, a variety of natively fluorescent biomolecules may be studied at the single-molecule level even though their fluorescence quantum yields and absorption coefficients are considerably lower than those of common fluorescent dyes. Biomolecules of particular interest include nicotinamide adenine dinucleotides, riboflavin, chlorophylls, porphyrins, and aromatic amino acids such as tryptophan.

The far-field confocal fluorescence approach has several advantageous features when compared with near-field optical microscopy, which achieves subwavelength resolution by sacrificing the excitation power throughput (32). With tapered single-mode fiber probes, the near-field power throughput is limited to \sim 50 nW for an 80-nm tip, and Trautman *et al.* (6) recently showed the necessity of integrating for sev-

Fig. 3 (left). Experimental and calculated fluorescence signals as a function of excitation power for single rhodamine 6G molecules in ethanol. The measured signal intensities are averaged values of 10 to 20 detection events and have an uncertainty error of \sim 10%. The photon absorption and emission cycle rate (k_f) of a single molecule is calculated by using the equation $k_f = 1/(\tau_f + 1/k_a)$, where τ_f is the excited state lifetime (\sim 3.4 ns), k_a is the absorption rate and is $3.8 \times 10^{-21} \epsilon P/\pi r_o^2$, where ϵ is the extinction coefficient, P is the laser excitation power, and r_o is the radius of the focused laser beam. This calculation gives the fluorescence cycle rate of a single molecule at a given power. The expected signal intensity can be calculated by multiplying the cycle rate by a constant factor that takes into account fluorescence quantum yield, intersystem crossing, and the combined detection efficiency [laser wavelength, 514.5 nm; emission bandpass filter, 560 nm



(FWHM 40 nm); and integration time per data point, 1.0 ms]. **Fig. 4 (right).** Time records of fluorescence emission of a single rhodamine 6G molecule in ethanol at different laser powers (514.5 nm). The probe volume was continuously monitored at a speed of 500,000 data points per second (2- μ s integration) until a burst of photons is detected; the fluorescence data were then stored for analysis.

eral minutes to obtain near-field fluorescence spectra with good signal-to-noise ratios. Furthermore, the recent work of Xie and Dunn (33) and by Ambrose *et al.* (34) showed that the metal-coated probe tip can significantly perturb the electronic properties of the molecule being detected. In contrast, the far-field confocal fluorescence approach provides unlimited laser throughput and a three-dimensional sectioning capability and is truly noninvasive, although its resolution is diffraction limited. These features are expected to allow important applications such as enhanced Raman spectroscopy at the single-molecule level and on-line fluorescence identification and sorting of individual molecules and quantum-confined nanostructures. The extraordinary sensitivity achieved in this work allows the direct, real-time study of the dynamics of a single molecule and the chemical and biochemical reactions that such a molecule may undergo in solution.

REFERENCES AND NOTES

- W. E. Moerner, *Science* **265**, 46 (1994), and references therein.
- M. Orrit, J. Bernard, R. I. Personov, *J. Phys. Chem.* **97**, 10256 (1993).
- F. Güttler, T. Irgartinger, T. Plakhotnik, A. Renn, U. P. Wild, *Chem. Phys. Lett.* **217**, 393 (1994).
- M. Ishikawa, K. Hirano, T. Hayakawa, S. Hosoi, S. Brenner, *Jpn. J. Appl. Phys.* **33**, 1571 (1994).
- E. Betzig and R. J. Chichester, *Science* **262**, 1422 (1993).
- J. K. Trautman, J. J. Macklin, L. E. Brus, E. Betzig, *Nature* **369**, 40 (1994).
- D. C. Nguyen, R. A. Keller, J. H. Jett, J. C. Martin, *Anal. Chem.* **59**, 2158 (1987).
- K. Peck, L. Stryer, A. N. Glazer, R. A. Mathies, *Proc. Natl. Acad. Sci. U.S.A.* **86**, 4087 (1989).
- W. B. Whitten, L. M. Ramsey, S. A. Arnold, B. V. Bronk, *Anal. Chem.* **63**, 1027 (1991); K. C. Ng, W. B. Whitten, S. A. Arnold, L. M. Ramsey, *ibid.* **64**, 2914 (1992).
- M. Eigen and R. Rigler, *Proc. Natl. Acad. Sci. U.S.A.* **91**, 5740 (1994).
- In fluorescence correlation spectroscopy, the intensity recorded at time t is multiplied by that recorded at $t + \Delta t$, and the product is integrated over a finite period of time; see D. E. Koppel, *Phys. Rev. A* **10**, 1938 (1974).
- T. T. Perkins, D. E. Smith, S. Chu, *Science* **264**, 819 (1994); T. T. Perkins, S. R. Quake, D. E. Smith, S. Chu, *ibid.*, p. 822.
- S. B. Smith, L. Finzi, C. Bustamante, *ibid.* **258**, 1122 (1992); C. Bustamante, *Annu. Rev. Biophys. Biochem. Phys. Chem.* **20**, 415 (1991).
- M. Washizu and O. Kurosawa, *IEEE Trans. Ind. Appl.* **26**, 1165 (1990).
- S. B. Smith, P. K. Aldridge, J. B. Callis, *Science* **243**, 203 (1989).
- N. J. Rampino and A. Chrambach, *Anal. Biochem.* **194**, 278 (1991).
- K. Morikawa and M. Yanagida, *J. Biochem.* **89**, 693 (1981).
- I. Auzanneau, C. Barreau, L. Salome, *C. R. Acad. Sci. Paris* **316**, 459 (1993).
- H. Kabata *et al.*, *Science* **262**, 1561 (1993).
- D. A. Schafer, J. Gelles, M. P. Sheetz, R. Landick, *Nature* **352**, 444 (1991).
- Laser excitation at 488.0 and 514.5 nm was provided by an argon ion laser (Lexel Lasers, Fremont, CA). The laser beam entered the microscope through a back port and was directed to an oil-immersion objective ($\times 100$, NA = 1.3, Nikon Instrument Group, Melville, NY) by a dichroic beamsplitter (505DRLP02 or 540DRLP02, Omega Optical Inc., Brattleboro, VT). The laser beam was focused to a diffraction-limited spot by the high NA objective in our study, which was verified qualitatively by comparing the laser focal size and 1- μm polystyrene microspheres (Duke Scientific, Palo Alto, CA). Fluorescence was collected by the same objective, passed the same dichroic beamsplitter, and was then directed to a side port by a reflective mirror. Efficient rejection of out-of-focus signals was achieved by placing a pinhole (50 to 100 μm diameter, Newport Corp., Irvine, CA) in the primary image plane. A single interference bandpass filter (Omega Optical Inc., Brattleboro, VT) was used to reject the laser light and the Rayleigh and Raman scattered photons. The fluorescence signal was then focused on a photon-counting Si avalanche photodiode (quantum efficiency, 55% at 630 nm, and dark noise, 7 counts per second) (Model SPCM-200, EG&G Canada, Vaudreuil, Quebec). Time-dependent data were acquired by using a multichannel scalar (EG&G ORTEC, Oak Ridge, TN) run on a personal computer (IBM PC-AT). Fluorescent dyes and other materials were purchased from Molecular Probes, Inc. (Eugene, OR), Eastman Chemicals (Kingsport, TN), and Sigma Chemical Corp. (St. Louis, MO).
- M. B. Schneider and W. W. Webb, *Appl. Opt.* **20**, 1382 (1981).
- R. Rigler, U. Mets, J. Widengren, P. Kask, *Eur. Biophys. J.* **22**, 169 (1993).
- W. Feller, *An Introduction to Probability Theory and its Applications* (Wiley, New York, ed. 3, 1968).
- S. A. Soper, H. L. Nutter, R. A. Keller, L. M. Davis, E. B. Shera, *Photochem. Photobiol.* **57**, 972 (1993).
- A complicating factor is photobleaching, which converts the molecule being detected into a nonfluorescent state and prevents its further detection. The multiple detection and similar fluorescence intensity observed for molecules of greatly different photodestruction efficiencies (that is, R6G and fluorescein) indicate however that photobleaching is not significant in this study.
- This calculation is based on the diffusion equation $\tau_D = \omega^2/2D$, where τ_D is the diffusion time, ω is the diffusion distance in one dimension, and D is the diffusion coefficient ($2.8 \times 10^{-6} \text{ cm}^2 \text{ s}^{-1}$ for rhodamine 6G in water/ethanol).
- D. Magde, E. L. Elson, W. W. Webb, *Biopolymers* **13**, 1 (1974); *ibid.*, p. 29.
- D. N. Dempster, T. Morrow, M. F. Quinn, *J. Photochem.* **2**, 343 (1973).
- M. M. Asimov, V. N. Gavrilenko, A. N. Rubinov, *J. Lumin.* **46**, 243 (1990).
- H. Qian and E. L. Elson, *Appl. Opt.* **30**, 1185 (1991).
- E. Betzig, J. K. Trautman, T. D. Harris, J. S. Weiner, R. L. Kostelak, *Science* **251**, 1468 (1991); E. Betzig and J. K. Trautman, *ibid.* **257**, 189 (1992).
- X. S. Xie and R. C. Dunn, *ibid.* **265**, 361 (1994).
- W. P. Ambrose, P. M. Goodwin, J. C. Martin, R. A. Keller, *ibid.*, p. 364.
- S.N. acknowledges the Whitaker Foundation for a young investigator award. D.T.C. is a Beckman Cell Science Scholar of Stanford University. This work was supported by Beckman Instruments, Inc.

18 July 1994; accepted 19 September 1994

Molecular Computation of Solutions to Combinatorial Problems

Leonard M. Adleman

The tools of molecular biology were used to solve an instance of the directed Hamiltonian path problem. A small graph was encoded in molecules of DNA, and the "operations" of the computation were performed with standard protocols and enzymes. This experiment demonstrates the feasibility of carrying out computations at the molecular level.

In 1959, Richard Feynman gave a visionary talk describing the possibility of building computers that were "sub-microscopic" (1). Despite remarkable progress in computer miniaturization, this goal has yet to be achieved. Here, the possibility of computing directly with molecules is explored.

A directed graph G with designated vertices v_{in} and v_{out} is said to have a Hamiltonian path (2) if and only if there exists a sequence of compatible "one-way" edges e_1, e_2, \dots, e_z (that is, a path) that begins at v_{in} , ends at v_{out} , and enters every other vertex exactly once. Figure 1 shows a graph that for $v_{\text{in}} = 0$ and $v_{\text{out}} = 6$ has a Hamiltonian path, given by the edges $0 \rightarrow 1, 1 \rightarrow 2, 2 \rightarrow 3, 3 \rightarrow 4, 4 \rightarrow 5, 5 \rightarrow 6$. If the edge $2 \rightarrow 3$ were removed from the graph, then the resulting graph with the same designated vertices would not have a Hamiltonian path. Similarly, if the designated vertices were changed to $v_{\text{in}} = 3$ and $v_{\text{out}} = 5$ there

would be no Hamiltonian path (because, for example, there are no edges entering vertex 0).

There are well-known algorithms for deciding whether an arbitrary directed graph with designated vertices has a Hamiltonian path or not. However, all known algorithms for this problem have exponential worst-case complexity, and hence there are instances of modest size for which these algorithms require an impractical amount of computer time to render a decision. Because the directed Hamiltonian path problem has been proven to be NP-complete, it seems likely that no efficient (that is, polynomial time) algorithm exists for solving it (2, 3).

The following (nondeterministic) algorithm solves the directed Hamiltonian path problem:

Step 1: Generate random paths through the graph.

Step 2: Keep only those paths that begin with v_{in} and end with v_{out} .

Step 3: If the graph has n vertices, then keep only those paths that enter exactly n vertices.

Step 4: Keep only those paths that enter all of

Department of Computer Science and Institute for Molecular Medicine and Technology, University of Southern California, 941 West 37th Place, Los Angeles, CA 90089, USA.